

T-Net: A Template-Supervised Network for Task-specific Feature Extraction in Biomedical Image Analysis

Weinan Song*, Yuan Liang*, Kun Wang*, and Lei He*

*University of California, Los Angeles, USA

Abstract—Existing deep learning methods depend on an encoder-decoder structure to learn feature representation from the segmentation annotation in biomedical image analysis. However, the effectiveness of feature extraction under this structure decreases due to the indirect optimization process, limited training data size, and simplex supervision method. In this paper, we propose a template-supervised network T-Net for task-specific feature extraction. Specifically, we first obtain templates from pixel-level annotations by down-sampling binary masks of recognition targets according to specific tasks. Then, we directly train the encoding network under the supervision of the derived task-specific templates. Finally, we combine the resulting encoding network with a posterior network for the specific task, e.g. an up-sampling network for segmentation or a region proposal network for detection. Extensive experiments on three public datasets (BraTS-17, MoNuSeg and IDRiD) show that T-Net achieves competitive results to the state-of-the-art methods and superior performance to an encoder-decoder based network. To the best of our knowledge, this is the first in-depth study to improve feature extraction by directly supervise the encoding network and by applying task-specific supervision in biomedical image analysis.

Index Terms—Deep learning, task-specific supervision, encoder-decoder network.

I. INTRODUCTION

Feature extraction plays a vital role in image analysis. In conventional methods, feature extraction is designed manually according to the topology structure, or the statistical information. Recently, with the rapid advance of deep learning, the feature extractor can be optimized automatically by training a deep neural network (DCNN) on large-scale labeled datasets, such as ImageNet [1] and COCO [2]. However, due to the tedious annotation work and professional knowledge requirement, most biomedical image datasets are notoriously small. Therefore, it is impractical to train a universal feature extractor for biomedical image analysis. Besides, the models that have been well trained on large-scale datasets, such as VGG [3] and ResNet [4], are difficult to be transferred to biomedical images as the physiological features can be different from those in general images. These two drawbacks have brought a great challenge for deploying such data-driven deep learning algorithms for automatic feature extraction in biomedical applications.

To solve this, many approaches for biomedical image analysis deploy an encoder-decoder structure to learn feature representation from the pixel-wise annotation. This architecture

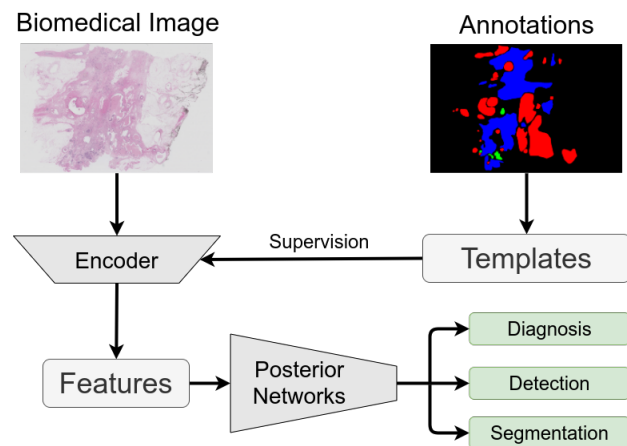


Fig. 1. An overview of T-Net structure. The encoding network learns feature representation with the supervision of templates, which are generated from the annotations via different down-sampling strategies. Then, the extracted features are taken as input of posterior networks for further analysis, e.g., pathological diagnosis, diseased organ detection, and abnormal tissue segmentation.

contains an encoder for extracting features from the input image and a decoder for up-sampling these features to generate segmentation output. The encoder and decoder can be achieved by two connected DCNNs, thus making the whole model a derivable mapping function that can be optimized by gradient descent based on the difference between the prediction and the segmentation ground truth. One of the most famous network is called U-Net, which has been widely used in many segmentation tasks. Under an encoder-decoder network, the feature representation can be automatically learned by the encoding network during the optimization process towards the specific loss function.

However, under such encoder-decoder structure, the gradient information can only be delivered to the encoding network after going through the decoding network during the training phase, even with skip-connections as short cuts. Therefore, optimizing the encoding network has to rely on the gradient information propagated from the decoding network. Moreover, since the decoding network usually has a mirror architecture of the encoding network, the encoder-decoder model usually has a strict restriction for the training image size due to the limited GPU memory, especially when processing high-

dimension and high-resolution images, *e.g.*, Magnetic Resonance Imaging (MRI) scans and computed tomography (CT) images. Furthermore, simply utilizing the binary segmentation mask as supervision has also limited the potential to optimize the feature representation. These three facts can decrease the feature extraction effectiveness of the encoding network, thus degrading the overall performance.

In this paper, we propose a template-supervised network, called T-Net, to improve the feature extraction effectiveness via templates. Our method is a general framework that can be adapted to different types of biomedical image problems. As shown in Fig. 1, we first generate templates from the binary mask of each recognition object by different down-sampling strategies. Then, we decouple the encoding network from the encoder-decoder structure and let the encoding network directly learn feature representation from the selected templates. Finally, we take the features extracted from the encoder as the input of posterior networks for further image analysis. To the best of our knowledge, this is the first in-depth study to improve the feature extraction effectiveness by decoupling the optimization process of the encoding network from the encoder-decoder structure and by applying templates as supervision in biomedical image analysis.

Compared with the encoder-decoder based feature extraction approaches, we show the advantages of T-Net in the following aspects:

- First, T-Net has a more concise architecture to optimize by removing the decoding network, which require much less memory footprint of GPU during the training phase. This can improve the learning efficiency of T-Net by training with larger patches when processing 3D data.
- Second, T-Net has a more straightforward way to optimize feature representation by deep supervision from the designed templates, where the gradient information can be directly propagated to the encoding network without going through the decoding network.
- Third, the supervision can be task-specific by adapting different strategies of template generation method. The feature extractor can put attention on different features when supervised by different templates.
- Fourth, T-Net can be viewed as a general framework to solve different types of tasks in biomedical image analysis. This can be achieved by combining the encoding network of T-Net with different posterior networks.

To show the effective feature extraction of T-Net, we do experiments for three different tasks in biomedical image analysis. We compare our framework with state-of-the-art methods, which are either top methods from the open leaderboard or the latest publications. To further prove the effectiveness of template supervision, we also include the result of a conventional encoder-decoder network to alleviate the architecture effect and do comparative studies to show the influence of different supervision strategies.

- **3D Segmentation:** We train T-Net to recognize three different parts of the tumor on the largest brain tumor MRI dataset. Benefit from removing the decoupling network, T-Net can be trained with the whole 3D image to learn

feature representation for different tumor areas. In this experiment, T-Net surpasses other single-stage models on the challenge leaderboard on overall segmentation performance.

- **2D Segmentation:** We deploy T-Net for 2D semantic nuclei segmentation on pathology images from multiple organs. T-Net is trained and evaluated by images from different groups, where the shape, size, and color of nuclei are much different from each other. In this experiment, T-Net outperforms other methods on the overall performance and achieves the best result when tested on the unseen images.
- **Localization:** We extend our framework to a localization task, which is a totally different task from the previous two experiments to show the extension ability. We first train the encoding network to learn feature representation of the optic disc (OD) in retinal fundus images. Then we train a detection network to predict coordinates of the OD center. In this experiment, T-Net outperforms the champion approach on the open leaderboard.

II. RELATED WORK

A. U-Net

Developed from FCN [5], U-Net [6] has proved to be the most famous encoder-decoder structure for semantic segmentation in biomedical applications. U-Net is a fully-automatic framework that consists of an encoding network to learn feature representation from the input image and a decoding network to produce segmentation results. These two networks have symmetrical architectures and are connected by skip connections between intermediate layers. 3D U-Net [7] extends the U-Net by introducing 3D convolution kernels and has shown promising performance on many volumetric segmentation tasks, *e.g.*, tumor segmentation [8] in MRI scans and whole heart segmentation [9] in CT images. For convenience, we refer to these 2D and 3D frameworks both as U-Net in this paper.

B. Task-specific U-Net

Many frameworks adapt U-Net for different applications by adding a task-specific network. They take U-Net as the backbone and train with pixel-wise, or volume-wise, annotations to learn feature representation of the recognition target for the encoding network. For example, UOLO [10] consists of U-Net as the object segmentation module, where the intermediate abstract representations are taken as the input of a region proposal network for landmarks detection in eye fundus images. Y-Net [11] adds a parallel branch at the bottom of U-Net to distinguish benign and malignant cancer in breast biopsy slices. Retina U-Net [12] fuses the one-stage detector with U-Net as the semantic segmentation supervision for lung lesion detection in CT images. DeepLung [13] utilizes U-Net to learn nodule features from lung 3D and do classification through gradient boosting machine with the extracted features. Compared with these frameworks, T-Net has a more concise architecture to learn feature representation by removing the decoding network. Besides, the supervision

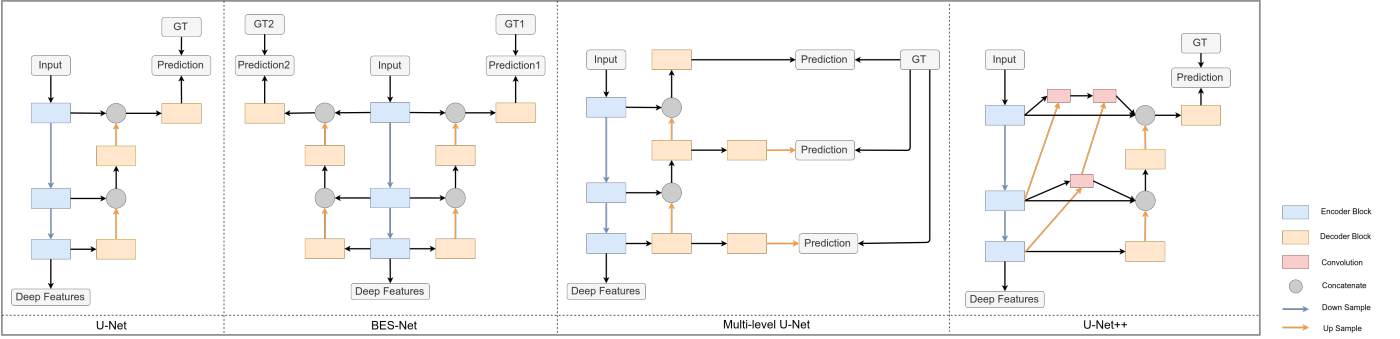


Fig. 2. We show examples of different deep supervision methods. Based on U-Net, these methods improve the feature representation effectiveness by increasing the model complexity. However, T-Net achieves this by directly supervising the encoding network with task-specific templates. Compared with these U-Net based models, our network has a more concise structure and can be easily adapted to different tasks.

method can be task-specific by adopting different template generation strategies. These features have made T-Net a plug-and-play framework and flexible to be generalized to different biomedical applications.

C. Deep Supervision for U-Net

Deep supervision is an efficient method to avoid gradient vanishing when training deep networks. Some work achieves this with an attention mechanism by supervising the network with additional information. For example, [14] takes the retinal vessel edge as additional class for a U-Net based segmentation problem. ES-Net [15] adds extra decoding network to learn the boundary information for cell segmentation. Other works improve the learning efficiency by modifying the supervision paths. For instance, U-Net++ [16] connects the encoding and decoding networks with a series of nested, dense skip pathways. Multi-level U-Net [17] up-samples multi-level features to establish connections directly with the ground truth. Some examples of these networks can be seen in Fig. 2, where we can see that these models still rely on an encoder-decoder structure. Compared with them, T-Net improves the learning efficiency in a different way by reducing the model complexity. We use template to directly supervise the encoding network and optimize the supervision object by adjusting template generation method.

III. METHODOLOGIES

A. Template

a) Learning from the Template: In T-Net, feature representation is learned directly from templates. The gradient information can be directly delivered to the encoding network, without going through the decoding network during the training phase. Here we take a one-class recognition problem for example, then training an encoder-decoder network to learn feature representation can be concluded as:

$$\min_{\theta_e, \theta_d} \text{Loss}(f_d(\theta_d, f_e(\theta_e, I)), I^B), \quad (1)$$

where I and I^B represent the input image and the binary mask of the recognition target, f_e and f_d represent the encoding and decoding network, and θ_e and θ_d represent the corresponding parameters of these two networks. The optimization is

achieved based on the gradient descent over θ_e and θ_d , which can be described as:

$$\begin{aligned} \frac{\partial \text{Loss}}{\partial \theta_e} &= \frac{\partial \text{Loss}}{\partial f_d} \cdot \frac{\partial f_d}{\partial f_e} \cdot \frac{\partial f_e}{\partial \theta_e}, \\ \frac{\partial \text{Loss}}{\partial \theta_d} &= \frac{\partial \text{Loss}}{\partial f_d} \cdot \frac{\partial f_d}{\partial \theta_d}. \end{aligned} \quad (2)$$

In T-Net, we introduce the template T and change the optimization problem (1) to:

$$\min_{\theta_e} \text{Loss}(f_e(\theta_e, I), T). \quad (3)$$

Then the gradient descent process in (2) is changed to:

$$\frac{\partial \text{Loss}}{\partial \theta_e} = \frac{\partial \text{Loss}}{\partial f_e} \cdot \frac{\partial f_e}{\partial \theta_e}. \quad (4)$$

By introducing templates, we change the optimization problem (1) into another optimization problem (3), where the optimization objective is deeply influenced by the templates we choose. This means that improper templates can supervise the network to learn feature representation in a wrong direction. Therefore, the key point is what should the encoding network expect to learn from for the specific biomedical analysis task.

b) Designing the Template: Our template design is inspired by the work of feature visualization [18], where filters in high *convolution* layers have a higher possibility to represent object parts. [19] also shows that the localization ability of DCNN trained from image-level annotations comes from the activation map of deep features. To this end, we can assume that deep features can be seen as partial representations of the recognition object. Therefore, we can simply utilize a probability map that represents the shape and spatial information of the recognition target in pixel level to supervise the feature extractor. Then the optimization problem of feature extraction becomes a feature-level linear regression problem about how to map the deep features generated by the last layer of the encoding network into this probability map. This can be solved by adding a *bottleneck* layer followed by a Sigmoid function at the bottom of the encoding network.

Till now, the template design becomes generating a probability map that reflects the shape and spatial information of the recognition object. Moreover, the probability map should also be able to match the size of deep features. Therefore,

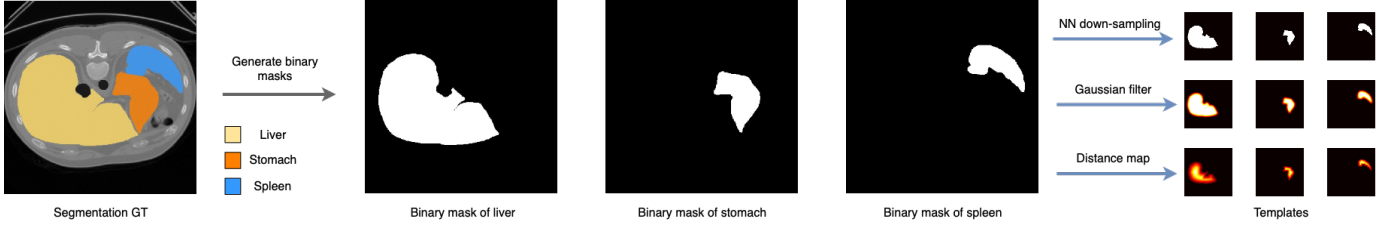


Fig. 3. Illustration of template generation with three down-sampling methods. We first obtain binary masks of the three recognition organs from the annotation. Then we apply NN down-sampling, Gaussian filter, and distance map to generate templates for each organ. From the results on the right side, we can clearly see the difference among these templates around the object boundary.

this problem can be seen as finding a down-sampling method $f_{template}$ denoted by:

$$f_{template} : I_{H_I \times W_I}^B \rightarrow T_{H_T \times W_T}, \quad (5)$$

which maps the binary image I^B with a size of $H_I \times W_I$ to a probability map with a size of $H_T \times W_T$. Note that this probability map is actually the template T we want.

Below we propose three methods to achieve $f_{template}$. These three strategies show different areas of the recognition target that we want the feature extractor to pay attention to. To be noted, the template generation is not limited to these three methods. We can also deploy other types of templates for supervision depending on specific applications.

(1) **NN Template:** The most intuitive way to generate templates is by directly down-sampling the binary mask of the recognition target with nearest-neighbor interpolation. This can guarantee that T can keep both the spatial and shape information of the recognition target and each pixel value in the template is either 0 or 1. We refer to the template generated by this method as NN template and show extensions of this template in the following content.

(2) **Gaussian Template:** To make the encoding network pay additional attention to the area outside the boundary of targets, we expand the NN template by applying a normalized Gaussian filter with a stride s . The Gaussian filter can make a smooth transition from foreground to background on the object boundary and the normalization can guarantee each pixel value in T is between 0 and 1. This can supervise the network to pay additional attention to the boundary area around the recognition target.

(3) **Distmap Template:** To encourage the encoding network to focus on the object center, we transform the NN template into a normalized distance map. In a distance map, each pixel value inside the object reflects the distance between it and the object boundary. For normalization, we divide the distance map by the largest distance value, which should belong to the center point as it is most far away from the background. We call this kind of template as the Distmap template and show the detail generation process in Algorithm 1, where α can adjust the decreasing speed of the normalized distance value from the center to the boundary.

For clearly illustrating the process of template generation, we show an example of generating these three types of templates for three recognition objects in Fig. 3. In this case, three abdomen organs, i.e., liver, stomach, and spleen, are annotated in a CT image. We first obtain binary masks

Algorithm 1 Generate the Distmap Template

```

1: function DISTMAP_TEMPLATE( $I^B, s, \alpha$ )
2:    $I^B \leftarrow$  DOWNSAMPLE( $I^B, s$ )
3:    $distmap \leftarrow$  ZEROS_LIKE( $I^B$ )
4:    $p\_set \leftarrow$  COORDINATE( $I^B \geq 0.5$ )
5:    $n\_set \leftarrow$  COORDINATE( $I^B < 0.5$ )
6:    $len\_p \leftarrow$  LEN( $p\_set$ )
7:   for  $i = 0; i < len\_p; i++$  do
8:      $y, x \leftarrow p\_set[i]$ 
9:      $distmap[y][x] \leftarrow$  DISTANCE( $n\_set, (y, x)$ )
10:  end for
11:   $distmap \leftarrow distmap / \text{MAX}(distmap)$ 
12:   $template \leftarrow distmap^\alpha$ 
13:  return  $template$ 
14: end function

```

for these three organs and then apply different $f_{template}$ to generate templates.

B. T-Net Architecture

a) **Network Overview:** We show the detailed structure of T-Net, containing an up-sampling network for segmentation and a detection network for localization in Fig. 4. T-Net takes an encoding network as the backbone to extract multi-level features, which are later taken as the input of posterior networks for further analysis. The proposed network architecture is developed from Dense V-Net [20], which utilizes dense connections among layers to enhance the learning ability. To be noted, the posterior networks can be in other forms according to the specific analysis task. We choose these two types of posterior networks in this paper because segmentation and localization are two fundamental problems in biomedical image analysis.

b) **Dense Blocks:** Dense block [21] has proved to be an efficient structure to connect *convolution* layers in DCNN. The input features, extracted by upper layers, first go through a *convolution* layer and generate K higher-level features. Then these new features are concatenated with the old features to be taken as input of the next layer. As shown in Fig. 5, the dense block repeats this for N times until reaching the last layer, where all the features are concatenated together as input of a *bottleneck* layer to reduce the number of feature maps.

c) **Encoding Network:** The encoding network has two steps of down-sampling to extract features. The *convolution*

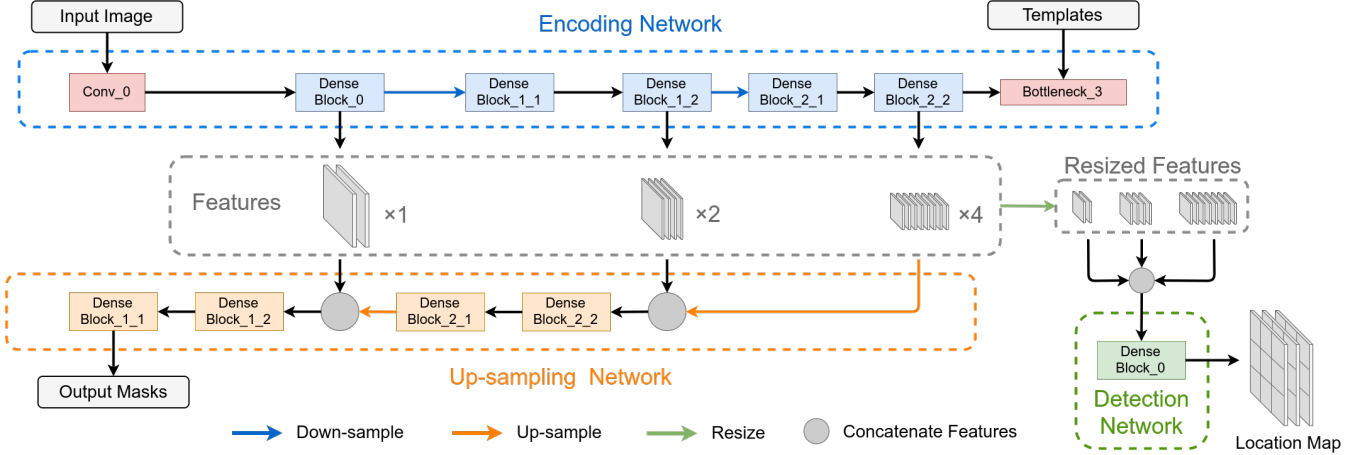


Fig. 4. The detailed architecture of T-Net, containing an up-sampling network for segmentation and a detection network for localization. The encoding network learns feature representation from templates, and generates $\times 1$, $\times 2$, $\times 4$ features as the input of posterior networks.

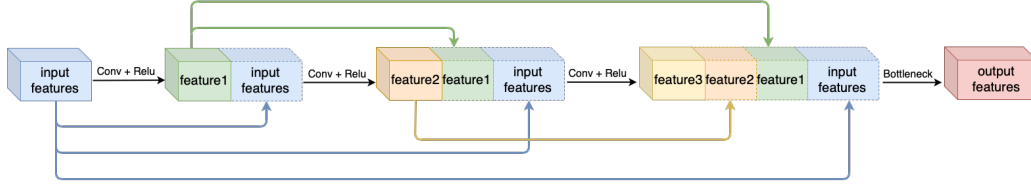


Fig. 5. An illustration of a dense block ($N = 3$) in T-Net.

layer on the top is responsible for mapping the input image into fixed-number feature maps. Then $\times 1$ features are generated from the first dense block, while $\times 2$ and $\times 4$ features are obtained from two consecutive dense blocks after a *max-pooling* layer. Finally, the $\times 4$ features are mapped into probability maps by the *bottleneck* layer activated by a Sigmoid function.

d) Up-sampling Network: The up-sampling network plays the same role as the decoding network in an encoder-decoder structure. Multi-level features generated by the encoding network are taken as input for up-sampling by transpose convolution. At the top of the up-sampling network, the features are finally transformed into binary masks for each segmentation object.

e) Detection Network: We use a similar way as [22] to design a detection network to predict the target location from the multi-level features extracted by the encoding network. The detection network first resizes these features into the same size as $H_L \times W_L$ by bilinear interpolation, then concatenates these resized features to be the input of a dense block to map them into a location map. The location map is a $H_L \times W_L \times C$ tensor that evenly divides the whole image into $H_L \times W_L$ cells. Then each vector at (i, j) in the location map indicates the detection result of the target whose center falls in the corresponding cell.

C. Loss Function.

a) Template Loss: Due to that the recognition object usually takes only a small part of the whole biomedical image, the loss function should consider the influence of the large area of background for the template regression. Therefore, we use

dice loss to optimize the encoding network of T-Net with N_T templates as:

$$Loss = 1 - \frac{1}{N_T} \sum_t \frac{2 \sum_i \sum_j p_{i,j,t} g_{i,j,t}}{\sum_i \sum_j p_{i,j,t}^2 + \sum_i \sum_j g_{i,j,t}^2}, \quad (6)$$

where $(p_{i,j,t}, g_{i,j,t})$ represents the prediction and ground truth input point pair for the t -th template. The dice loss reflects the ratio of the correct predictions and the union of all the positive predictions and the ground truth. It is always non-negative and can be 0 if and only if the model correctly predicts all the points.

b) Up-sampling Loss: Since the up-sampling network is mainly for segmentation, we can also use dice loss as in equation (6) to optimize the up-sampling network. The only difference is that $g_{i,j,t}$ is binary and N_T equals to the number of segmentation classes.

c) Location Loss: We use MSE loss, same as in [10], to optimize the detection network. In our experiment, since we only predict the center coordinates of OD, we can simply use (x, y, c) at (i, j) in the location map to represent the localization result. Here c is the confidence score indicating whether the corresponding cell contains the OD center and (x, y) represents the relative offsets. Then location loss can

TABLE I
DENSE BLOCK SETTINGS IN THREE EXPERIMENTS.

Name	Brain tumor segmentation								Nuclei segmentation								OD detection											
	Encoding Network				Up-sampling Network				Encoding Network				Up-sampling Network				Encoding Network				Detection Network							
	In	Out	K	N	In	Out	K	N	In	Out	K	N	In	Out	K	N	In	Out	K	N	In	Out	K	N				
Dense_0	16	16	8	4	-	-	-	-	16	16	8	3	-	-	-	-	16	16	8	4	112	3	16	4	-	-	-	-
Dense_1_1	16	32	8	4	16	3	8	4	16	32	8	3	16	1	8	3	16	32	8	4	-	-	-	-	-	-	-	-
Dense_1_2	32	32	8	4	48	16	8	4	32	32	8	3	48	16	8	3	32	32	8	4	-	-	-	-	-	-	-	-
Dense_2_1	32	64	8	4	32	32	8	4	32	64	8	3	32	32	8	3	32	64	8	4	-	-	-	-	-	-	-	-
Dense_2_2	64	64	8	4	96	32	8	4	64	64	8	3	96	32	8	3	64	64	8	4	-	-	-	-	-	-	-	-

be simplified as:

$$\begin{aligned}
 Loss = & \sum_i^{H_L} \sum_j^{W_L} w_{i,j} (c_{i,j} - \bar{c}_{i,j})^2 \\
 & + \sum_i^{H_L} \sum_j^{W_L} \mathbb{1}_{i,j}^{obj} \left[(x_{i,j} - \bar{x}_{i,j})^2 + (y_{i,j} - \bar{y}_{i,j})^2 \right], \quad (7)
 \end{aligned}$$

where \bar{c} and (\bar{x}, \bar{y}) are the groundtruth confidence score and offsets. Besides, we also introduce weight w to prevent the detection network from falling into local optimal. Given the object center in the (O_x, O_y) cell, the weight w can be calculated as:

$$w_{i,j} = \begin{cases} \frac{1}{H_L \times W_L} & else \\ \frac{1}{8} & |i - O_x| = 1 \text{ or } |j - O_y| = 1 \\ 1 & i = O_x \text{ and } j = O_y \end{cases} \quad (8)$$

IV. EXPERIMENTS

We evaluate our approach on three public datasets for three different tasks: (1) the BraTS-17 dataset [23] [24] for 3D brain tumor segmentation, (2) the MoNuSeg dataset [25] for 2D semantic nuclei segmentation, and (3) the IDRiD dataset [26] for OD localization. In these experiments, T-Net achieves competitive performance to the state-of-the-art methods. We show the performance of these three experiments in Table II-IV and visualize some results in Fig. 6-8.

A. Experiment Settings

We first train the encoding network with proposed template and then train the posterior network with a fixed encoding network. Specifically, we can also train the posterior networks without fixing the encoding network, but that is beyond our topic and we will put in our future work. We train both networks for 100 epochs in tumor segmentation and 500 epochs for both networks in the rest two experiments. For the Gaussian template, we set the filter window to be 12 on each dimension. For the Distmap template, we use Chebyshev distance and set α to be 2. The detail structure of T-Net for each experiment can be seen in Table I. For OD localization, we set $H_L \times W_L$ to be 32×48 . For optimization, we use Adam [27] optimizer with a learning rate of 10^{-4} for each network.

B. Validation of T-Net.

a) **Template Selection:** For tumor segmentation, we choose NN template to keep the shape of different tumor areas. For nuclei segmentation, we utilize Gaussian template to expand the attention space to the outside boundary. For OD localization, we use Distmap template to make the network focus on the object center. We compare the results with other methods can be seen in Table II - IV.

b) **Comparative Studies:** To show the improvement from the template supervision and alleviate the influence by the network architecture, we also train an encoder-decoder network, named as baseline U-Net, with the same settings as T-Net (except with no templates) for each experiment. The baseline U-Net learns feature representation only from the segmentation ground truth. It is achieved by directly connecting the encoding and the up-sampling networks in the first two experiments and adding a symmetrical decoding network in the last experiment. Additionally, to compare the influence brought by the template selection, we also supervise the encoding network with the other two templates. The overall performance can be seen in Table V.

C. Dataset and Tasks

a) **BraTS for 3D Tumor Segmentation:** Automatic brain tumor segmentation is one of the most challenging medical challenges since the tumor, together with its surroundings, is often diffused, poorly-contrasted, and extends tentacle-like structures. We use the BraTS-17 dataset for brain tumor segmentation to evaluate the performance of T-Net. The dataset contains 285 cases for training and 46 cases for online validation. Each case contains T1, T1Gd, T2, and FLAIR MRI images with annotations for the edema, the enhancing tumor (ET), and the non-enhancing tumor & the necrotic. The segmentation objective is to label the whole tumor (WT), the tumor core (TC) and the ET areas, respectively. The segmentation is evaluated by the unseen validation data online over dice score (%) and 95% Hausdorff distance (mm), which are criterions in the official challenge. We also use a score $S = \sum_{class} (Dice/200 - Hausdorff/60)$, to reflect the overall performance.

b) **MoNuSeg for 2D Nuclei Segmentation:** Nuclei are the most important biomedical elements to be segmented in pathology tissue slides as they are indicative of many cellular phenotypes. In this experiment, we evaluate the generalization

TABLE II
EVALUATION ON BRAIN TUMOR SEGMENTATION.

Method	Dice			Hausdorff			S
	WT	TC	ET	WT	TC	ET	
Sequential U-Net [28]	88.2	73.2	73.0	8.12	11.4	6.17	0.74
3D FCN [29]	89.9	75.1	71.3	4.16	8.65	6.98	0.85
Residual U-Net [8]	89.6	79.7	73.2	6.97	9.48	4.55	0.86
T-Net	88.9	76.7	71.5	4.86	8.20	4.46	0.89

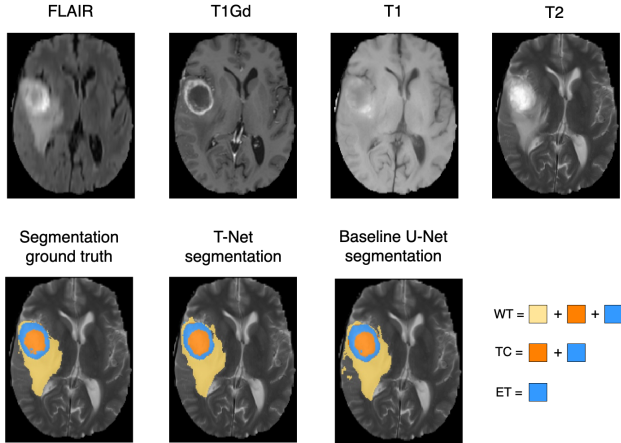


Fig. 6. Comparison of T-Net and the baseline U-Net for brain tumor segmentation.

TABLE III
EVALUATION ON MULTI-ORGAN NUCLEI SEGMENTATION.

Method	Test A	Test B	Overall
Dist U-Net [30]	0.7756	0.8005	0.7863
RIC U-Net [31]	-	-	0.8008
FullNet [32]	0.8007	0.8054	0.8027
T-Net	0.7930	0.8346	0.8108

ability of T-Net by deploying it for semantic nuclei segmentation on the MoNuSeg dataset, which contains $30\,1000 \times 1000$ H&E stained tissue images with hundreds of labeled nuclei from seven organs, i.e., breast, kidney, liver, prostate, bladder, colon, and stomach. We refer the first four organs as organ group A and the last three as organ group B, where the shape, size, and color of nuclei are much different from those in group A. The dataset is split into three parts with the same way in [25]: (1) 12 images from the organ group A for training and other 4 images for validation, (2) 8 images from the organ group A for test A, and (3) 6 images from the organ group B for test B. The segmentation is evaluated by the average dice coefficient (ADC).

c) **ODRid for OD Localization**: OD localization is vital as it is the landmark of retinal fundus photographs. Here, we use IDRid dataset to evaluate T-Net for predicting the coordinates of OD center. The dataset consists of a segmentation group, containing 81 images with pixel-level annotations, and a localization group, containing 516 images (413 for training and 103 for test) only with the coordinate information of OD center. The localization is evaluated mean Euclidean distance

TABLE IV
EVALUATION FOR OD LOCALIZATION.

Method	ED
RPI-based faster RCNN [33]	32.60
Relation Net [34]	26.12
Leaderboard Champion	25.62
T-Net	24.85

TABLE V
COMPARE THE OVERALL PERFORMANCE OF T-NET SUPERVISED BY DIFFERENT TEMPLATES AND THE BASELINE U-NET.

Method	Template	BraTS	MoNuSeg	ODRid
Baseline U-Net	-	0.85	0.7987	32.61
T-Net	NN	0.89	0.8028	42.10
T-Net	Gaussian	0.76	0.8108	34.21
T-Net	Distmap	0.83	0.8066	24.85

(ED) between the prediction and ground truth.

D. Discussion

a) **Comparison with state-of-the-art methods**: We compare T-Net with state-of-the-art methods and show the results in Table II-IV. We can see that T-Net can achieve the best performance, compared to the state-of-the-art methods in each experiment. For tumor segmentation, T-Net surpasses Res U-Net, which is the top single-stage model on the challenge leaderboard, with an overall score at 0.89 vs 0.85. The drop on dice scores of TC and ET mainly comes from the cases that have no TC and ET areas, where only one positive prediction can bring the dice score from 1 to 0. For nuclei segmentation, T-Net significantly surpasses other methods on images from unseen organs (0.8364 vs 0.8054 for FullNet). For OD localization, T-Net outperforms the champion approach on the open leaderboard (24.85 vs 25.62).

b) Comparison among different supervision methods

We also supervise T-Net with the other two templates in each experiment to indicate the importance of choosing the correct templates. As shown in Table V, the selection of templates can influence the performance for different tasks. That is quite intuitive as a teacher can not expect students to achieve good grades if he teaches them wrong knowledge. For example, if we train T-Net supervised with Distmap templates for brain tumor segmentation, it would show poor performance as the encoding network cannot learn enough shape information from the templates for each tumor.

c) Comparison with the baseline U-Net

From Table V we can see that T-Net supervised with the correct task-specific templates can always beat the baseline U-Net in the three experiments. This indicates the effectiveness of T-Net over the encoder-decoder network. In the first experiment, the baseline U-Net is trained with a patch size of 96^3 , which is the largest we can fit our GPU (Titan Xp). Therefore, the improved performance of T-Net mainly comes from the concise architecture, where the encoding and decoding networks can be trained separately. For nuclei segmentation, T-Net can pay additional attention to the boundary areas of nuclei with the

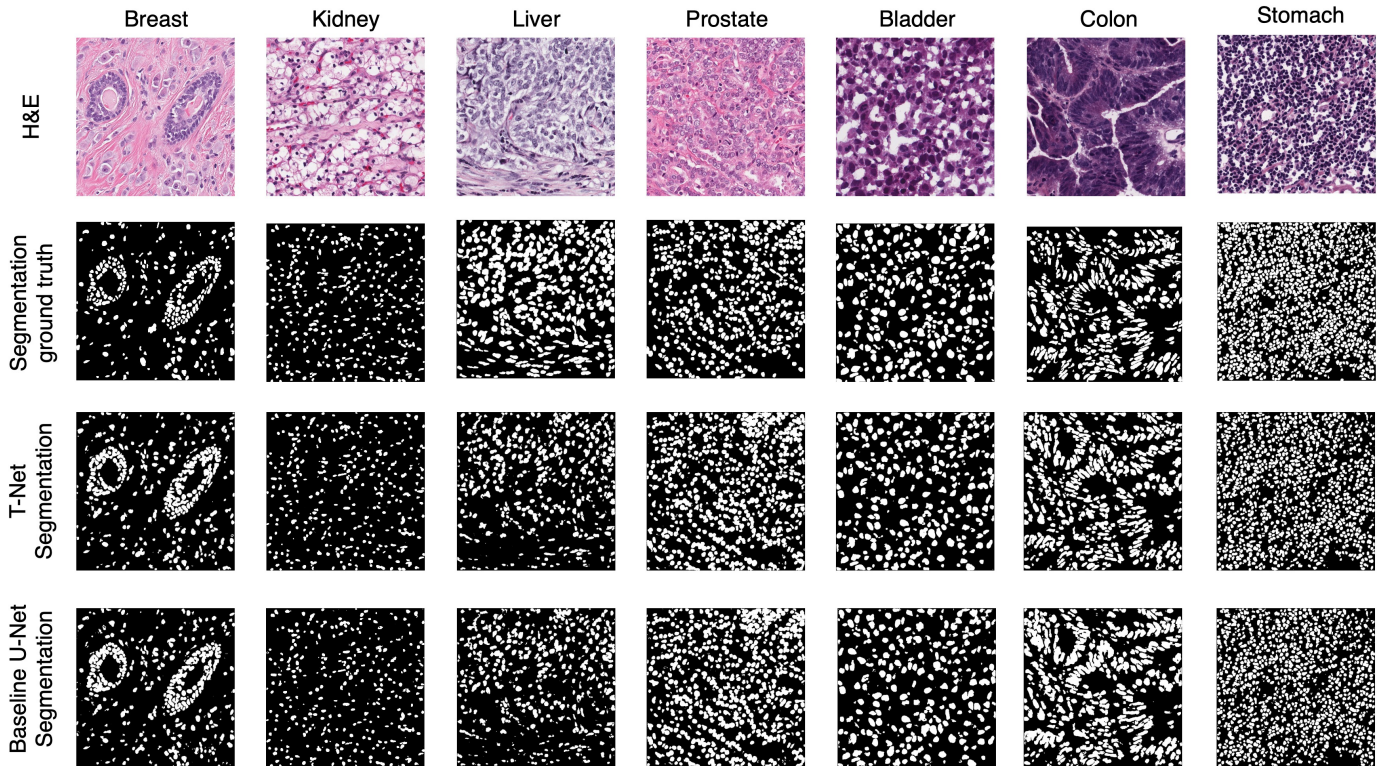


Fig. 7. Comparison of T-Net and the baseline U-Net for multi-organ nuclei segmentation.

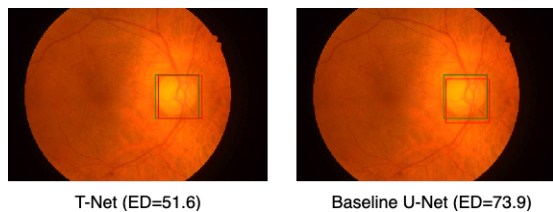


Fig. 8. T-Net outperforms the baseline U-Net for OD localization, shown by fixed-size bounding boxes, where prediction is in red and ground truth in green.

supervision of Gaussian templates. For OD localization, T-Net can focus on the center area when the Dismap template is applied. These experiments have shown the advantage of our proposed task-specific supervision method.

V. CONCLUSIONS

In this paper, we have proposed a novel deep supervision method by directly training the encoding network with task-specific templates to improve feature extraction for biomedical image analysis. T-Net removes the decoder from the encoder-decoder network (e.g., U-Net), but applies templates to supervise the encoder for feature extraction, where templates are generated from binary masks of recognition targets. Extensive experiments on three public datasets: BraTS-17, MoNuSeg, and IDRiD, show that T-Net can achieve superior performance compared with conventional encoder-decoder networks, thus indicating the effectiveness of our supervision method. The framework of T-Net is also general and extendable, as T-Net

is applicable to tasks of different characteristics and easy to be optimized by supervision of task-specific templates.

REFERENCES

- [1] J. Deng, W. Dong, R. Socher, L.-J. Li, K. Li, and L. Fei-Fei, “Imagenet: A large-scale hierarchical image database,” in *2009 IEEE conference on computer vision and pattern recognition*. Ieee, 2009, pp. 248–255.
- [2] T.-Y. Lin, M. Maire, S. Belongie, J. Hays, P. Perona, D. Ramanan, P. Dollár, and C. L. Zitnick, “Microsoft coco: Common objects in context,” in *European conference on computer vision*. Springer, 2014, pp. 740–755.
- [3] K. Simonyan and A. Zisserman, “Very deep convolutional networks for large-scale image recognition,” *arXiv preprint arXiv:1409.1556*, 2014.
- [4] K. He, X. Zhang, S. Ren, and J. Sun, “Deep residual learning for image recognition,” in *Proceedings of the IEEE conference on computer vision and pattern recognition*, 2016, pp. 770–778.
- [5] J. Long, E. Shelhamer, and T. Darrell, “Fully convolutional networks for semantic segmentation,” in *Proceedings of the IEEE conference on computer vision and pattern recognition*, 2015, pp. 3431–3440.
- [6] O. Ronneberger, P. Fischer, and T. Brox, “U-net: Convolutional networks for biomedical image segmentation,” in *International Conference on Medical image computing and computer-assisted intervention*. Springer, 2015, pp. 234–241.
- [7] Ö. Çiçek, A. Abdulkadir, S. S. Lienkamp, T. Brox, and O. Ronneberger, “3d u-net: learning dense volumetric segmentation from sparse annotation,” in *International conference on medical image computing and computer-assisted intervention*. Springer, 2016, pp. 424–432.
- [8] F. Isensee, P. Kickingereder, W. Wick, M. Bendszus, and K. H. Maier-Hein, “Brain tumor segmentation and radiomics survival prediction: contribution to the brats 2017 challenge,” in *MICCAI Brainlesion Workshop*. Springer, 2017, pp. 287–297.
- [9] Q. Tong, M. Ning, W. Si, X. Liao, and J. Qin, “3d deeply-supervised u-net based whole heart segmentation,” in *International Workshop on Statistical Atlases and Computational Models of the Heart*. Springer, 2017, pp. 224–232.
- [10] T. Araújo, G. Aresta, A. Galdran, P. Costa, A. M. Mendonça, and A. Campilho, “Uolo-automatic object detection and segmentation in biomedical images,” in *Deep Learning in Medical Image Analysis and*

- Multimodal Learning for Clinical Decision Support*. Springer, 2018, pp. 165–173.
- [11] S. Mehta, E. Merca, J. Bartlett, D. Weaver, J. G. Elmore, and L. Shapiro, “Y-net: joint segmentation and classification for diagnosis of breast biopsy images,” in *International Conference on Medical Image Computing and Computer-Assisted Intervention*. Springer, 2018, pp. 893–901.
 - [12] P. F. Jaeger, S. A. Kohl, S. Bickelhaupt, F. Isensee, T. A. Kuder, H.-P. Schlemmer, and K. H. Maier-Hein, “Retina u-net: Embarrassingly simple exploitation of segmentation supervision for medical object detection,” *arXiv preprint arXiv:1811.08661*, 2018.
 - [13] W. Zhu, C. Liu, W. Fan, and X. Xie, “Deeplung: Deep 3d dual path nets for automated pulmonary nodule detection and classification,” in *2018 IEEE Winter Conference on Applications of Computer Vision (WACV)*. IEEE, 2018, pp. 673–681.
 - [14] Y. Zhang and A. C. Chung, “Deep supervision with additional labels for retinal vessel segmentation task,” in *International conference on medical image computing and computer-assisted intervention*. Springer, 2018, pp. 83–91.
 - [15] H. Oda, H. R. Roth, K. Chiba, J. Sokolić, T. Kitasaka, M. Oda, A. Hinoki, H. Uchida, J. A. Schnabel, and K. Mori, “Besnet: Boundary-enhanced segmentation of cells in histopathological images,” in *International Conference on Medical Image Computing and Computer-Assisted Intervention*. Springer, 2018, pp. 228–236.
 - [16] Z. Zhou, M. M. R. Siddiquee, N. Tajbakhsh, and J. Liang, “Unet++: A nested u-net architecture for medical image segmentation,” in *Deep Learning in Medical Image Analysis and Multimodal Learning for Clinical Decision Support*. Springer, 2018, pp. 3–11.
 - [17] G. Zeng, X. Yang, J. Li, L. Yu, P.-A. Heng, and G. Zheng, “3d u-net with multi-level deep supervision: fully automatic segmentation of proximal femur in 3d mr images,” in *International workshop on machine learning in medical imaging*. Springer, 2017, pp. 274–282.
 - [18] Q. Zhang, Y. Wu, and S.-C. Zhu, “Interpretable convolutional neural networks,” in *Proceedings of the IEEE Conference on Computer Vision and Pattern Recognition*, 2018, pp. 8827–8836.
 - [19] B. Zhou, A. Khosla, A. Lapedriza, A. Oliva, and A. Torralba, “Learning deep features for discriminative localization,” in *Proceedings of the IEEE conference on computer vision and pattern recognition*, 2016, pp. 2921–2929.
 - [20] E. Gibson, F. Giganti, Y. Hu, E. Bonmati, S. Bandula, K. Gurusamy, B. Davidson, S. P. Pereira, M. J. Clarkson, and D. C. Barratt, “Automatic multi-organ segmentation on abdominal ct with dense v-networks,” *IEEE transactions on medical imaging*, vol. 37, no. 8, pp. 1822–1834, 2018.
 - [21] G. Huang, Z. Liu, L. Van Der Maaten, and K. Q. Weinberger, “Densely connected convolutional networks,” in *Proceedings of the IEEE conference on computer vision and pattern recognition*, 2017, pp. 4700–4708.
 - [22] J. Redmon and A. Farhadi, “Yolo9000: better, faster, stronger,” in *Proceedings of the IEEE conference on computer vision and pattern recognition*, 2017, pp. 7263–7271.
 - [23] B. H. Menze, A. Jakab, S. Bauer, J. Kalpathy-Cramer, K. Farahani, J. Kirby, Y. Burren, N. Porz, J. Slotboom, R. Wiest *et al.*, “The multimodal brain tumor image segmentation benchmark (brats),” *IEEE transactions on medical imaging*, vol. 34, no. 10, pp. 1993–2024, 2015.
 - [24] S. Bakas, H. Akbari, A. Sotiras, M. Bilello, M. Rozycki, J. S. Kirby, J. B. Freymann, K. Farahani, and C. Davatzikos, “Advancing the cancer genome atlas glioma mri collections with expert segmentation labels and radiomic features,” *Scientific data*, vol. 4, p. 170117, 2017.
 - [25] N. Kumar, R. Verma, S. Sharma, S. Bhargava, A. Vahadane, and A. Sethi, “A dataset and a technique for generalized nuclear segmentation for computational pathology,” *IEEE transactions on medical imaging*, vol. 36, no. 7, pp. 1550–1560, 2017.
 - [26] P. Porwal, S. Pachade, R. Kamble, M. Kokare, G. Deshmukh, V. Sahasrabudhe, and F. Meriaudeau, “Indian diabetic retinopathy image dataset (idrid): a database for diabetic retinopathy screening research,” *Data*, vol. 3, no. 3, p. 25, 2018.
 - [27] D. P. Kingma and J. Ba, “Adam: A method for stochastic optimization,” *arXiv preprint arXiv:1412.6980*, 2014.
 - [28] A. Beers, K. Chang, J. Brown, E. Sartor, C. Mammen, E. Gerstner, B. Rosen, and J. Kalpathy-Cramer, “Sequential 3d u-nets for biologically-informed brain tumor segmentation,” *arXiv preprint arXiv:1709.02967*, 2017.
 - [29] A. Jesson and T. Arbel, “Brain tumor segmentation using a 3d fcn with multi-scale loss,” in *International MICCAI Brainlesion Workshop*. Springer, 2017, pp. 392–402.
 - [30] P. Naylor, M. Laé, F. Reyat, and T. Walter, “Segmentation of nuclei in histopathology images by deep regression of the distance map,” *IEEE transactions on medical imaging*, vol. 38, no. 2, pp. 448–459, 2019.
 - [31] Z. Zeng, W. Xie, Y. Zhang, and Y. Lu, “Ric-unet: An improved neural network based on unet for nuclei segmentation in histology images,” *IEEE Access*, vol. 7, pp. 21 420–21 428, 2019.
 - [32] H. Qu, Z. Yan, G. M. Riedlinger, S. De, and D. N. Metaxas, “Improving nuclei/gland instance segmentation in histopathology images by full resolution neural network and spatial constrained loss,” in *International Conference on Medical Image Computing and Computer-Assisted Intervention*. Springer, 2019, pp. 378–386.
 - [33] X. Li, L. Shen, and J. Duan, “Optic disc and fovea detection using multi-stage region-based convolutional neural network,” in *Proceedings of the 2nd International Symposium on Image Computing and Digital Medicine*, 2018, pp. 7–11.
 - [34] S. C. Babu, S. R. Maiya, and S. Elango, “Relation networks for optic disc and fovea localization in retinal images,” *arXiv preprint arXiv:1812.00883*, 2018.